Polymer Testing 109 (2022) 107553

Contents lists available at ScienceDirect

Polymer Testing

journal homepage: www.elsevier.com/locate/polytest

# Development of hydro-axial tension method for whole pipe butt-fusion joint tensile test

Pyeong An Lee [a], Sunwoo Kim [a,b], Bob Stakenborghs [c], Yeongsung Suh [d], Sunwoong Choi [a,*]

[a] Department of Polymer Science and Engineering, Hannam University, Daejeon, 34054, South Korea
[b] Korea Research Institute of Chemical Technology, Daejeon, 34114, South Korea
[c] Advanced Microwave Imaging, Baton Rouge, LA, 70815, USA
[d] Department of Mechanical Engineering, Hannam University, Daejeon, 34430, South Korea

ARTICLE INFO

*Keywords:*
Polyethylene pipe
Hydro-axial tension test
Whole pipe axial tensile test
Butt-fusion joint
Cold fusion
Fine particulate contamination

ABSTRACT

Assessing the integrity of the thermo-fusion joint in plastic pipes is important as they can appear as a weak link in the piping system. In this work, a hydro-axial tension (HAT) test was developed as a whole pipe axial tensile test and applied to evaluate the polyethylene (PE) pipe butt-fusion (BF) joint containing various flaws. HAT test utilizes hydrostatic pressure to cause axial tension in pipes. The experimental and numerical analysis was carried out to confirm the axial tensile stress as the dominant principal stress, causing axial tension in the pipe. The HAT method was further tested against the whole pipe mechanical axial tensile (AT) test, and the HAT was shown to closely duplicate the AT behavior of the whole pipe and the BF joint. In addition, the HAT test correctly identified PE pipe butt-fusions having no flaws and flawed joints containing cold-fusion and fine particulate contamination.

## Author statement

Pyeong An Lee: Conceptualization, Methodology, Validation, Formal analysis, Investigation, Data Curation. Sunwoo Kim: Validation, Formal analysis, Data Curation. Bob Stakenborghs: Conceptualization, Investigation, Data Curation, Writing - Review & Editing. Yeongsung Suh: Formal analysis, Writing - Review & Editing. Sunwoong Choi: Conceptualization, Methodology, Formal analysis, Writing - Original Draft, Writing - Review & Editing, Supervision, Project administration, Funding acquisition.

## 1. Introduction

Plastic pipes are now well accepted as an integral part of fluid conveyance systems and are widely used in oil, gas, water, and industrial fluid transport. More demanding applications are emerging where higher pressure and larger diameter requirements are on the agenda [1–4]. Among them, nuclear industries have developed an ASME B&PV code section to include the use of high-density polyethylene (PE-HD) piping for safety Class 3 applications [5]. These emerging applications are often the result of the unparalleled mechanical and physical properties that the newly developed plastic materials for pipings are capable of delivering. They offer higher safety and cost-effectiveness in terms of ease of installation, use in rigorous conditions (e.g., toxic soil and seismic loading), and are almost free of long-term maintenance (e.g., galvanic corrosion and tuberculation) [6–10]. This, along with the excellent long years of safety record offered, plastic pipes are becoming the choice for replacing conventional material pressure pipes. One of the challenges faced when using plastic pipes in such demanding applications is the assurance of the joint integrity of the piping system. Joints are considered the weakest link in any piping system, and delivering leak-free performance is of utmost importance. Extensive destructive and non-destructive testing is being carried out to demonstrate their structural integrity. Two of the most popular plastic pipe jointing methods are butt-fusion (BF) [11,12] and electrofusion (EF) jointing [11,13,14], and their choice is mostly based on installation accessibility and pipe size. Both are thermal-fusion jointing, activated by the auto-adhesion mechanisms [15–17]. Thus any hindrances to auto-adhesion, such as cold fusion (CF), fine particulate contamination (FPC), planar flaws, are all known to reduce fusion joint integrity. Several test methods are available for determining the integrity of fusion joints [8,11,18–26]. However, most of them are based on coupon tests, where the specimens are locally removed and tested as a single entity with a limited portion of the actual fusion joint included [8,11,23–25]. Thus, if the flawed portion of the fusion joint is missed in the cut out from the pipe circumference, an erroneous assessment of the fusion joint can occur. The advantage of doing a whole pipe BF tensile test is evident

* Corresponding author.
*E-mail address:* swchoi@hnu.kr (S. Choi).

https://doi.org/10.1016/j.polymertesting.2022.107553
Received 13 December 2021; Received in revised form 5 March 2022; Accepted 20 March 2022
Available online 22 March 2022

**Abbreviations**

| | |
|---|---|
| AT | axial tensile |
| BF | butt-fusion |
| CF | cold fusion |
| COT | change over time |
| EF | electrofusion |
| FE | finite element |
| FPC | fine particulate contamination |
| HAT | hydro-axial tension |
| PE-HD | high-density polyethylene |
| LOF | lack of fusion |
| NH | no hole |
| NI | no flaw |
| P | pipe |
| SDR | standard dimensional ratio |
| WH | with holes |
| E.g., HAT-BF–NI–WH | hydro-axial tension-butt fusion-no flaw-with holes |

in that this would represent an actual test of the entire BF joints in the pipe system as a whole. Thus in a whole pipe tensile test, the interaction between the normal and flawed portion, if they co-exist in the BF, is tested together and evaluated. The whole pipe fusion joint tensile test would be of much value in the qualification of installation procedures where butt-fused pipes are pulled axially with a large force, and fusion joint integrity must be assured. This is particularly true, for example, in butt-fused piping that is axially pulled as part of the installation process, such as in horizontal directional drilling or pipe bursting. At present, only a couple of tests exist for subjecting the whole pipe fusion joint to tensile test conditions. Both axial tensile pull [27,28] and push-type [29] of kinematics are available. The push-type applies axial tension to the fusion joint by pushing a rod in contact with the inner surface of an end cap using a hydraulic cylinder. Push-type has a pipe size limitation for whole pipe tensile testing. On the other hand, the pull-type uses pipe end grips to apply axial tensile force to the whole pipe, requiring a large-capacity vertical or horizontal tensioning device [28,30] as the pipe size is increased. More recently, to alleviate the problems associated with the above described mechanical whole pipe axial tension devices, Wermelinger [31] and Choi [32,33] independently developed the whole pipe axial tension test using internal hydrostatic pressure (hydro-axial tension (HAT) test) and successfully applied for studying the effect of various flaws on the long-term performance of polyethylene BF joints. Choi went on to show that the HAT stress-rupture results were in good agreement with the whole pipe axial tensile (AT) stress-rupture test on 110 SDR 9 BF joints performed using mechanical loading. Wermelinger further applied the HAT method to BF and EF joints and developed stress-rupture curves for performance assessment of BF and EF joints containing planar flaws of various sizes and shapes. The advantage of using the HAT test over AT test for the whole pipe axial tension test is that the HAT test allows similar pressure to generate axial pipe tension for the same standard-dimension-ratio (SDR) pipe size, independent of the pipe diameter. It is noted that with the same SDR, an increase in pipe size similarly increases the axial tension on the pipe wall thickness, hence producing the same axial tensile stress on the pipe wall. On the other hand, as mentioned before, the AT test would require an increasingly higher axial load with increasing nominal diameter and decreasing SDR, making the experiment exceedingly difficult to perform. The HAT test developed by Wermelinger [31] and Choi [32,33] is based on the end-cap mass or steel clamping that provides restraint to hoop expansion during pipe internal pressure application. This would cause axial displacement on the pipe in the gap between two end-cap masses or steel clamps, where the BF bead resides. However, the use of these methods is limited as it pertains to evaluating the slow crack growth failures, where the overall long-term creep displacement due to the sustained internal pressure loading is maintained small. As the distance between the gap gets larger than three times, the BF bead width hoop tension again takes over as the main tensile force [34], and the test becomes no longer a whole pipe axial tensile test. This paper describes the development of the HAT test for performing a large displacement axial tensile test on the whole pipe. The background of development, experimental and numerical analysis, and the HAT method for the integrity assessment of whole pipe BF joints containing various flaws are described and compared to the AT method.

## 2. Development of whole pipe hydro-axial tension test

### 2.1. Background

When the hydrostatic internal pressure is applied in an end-capped

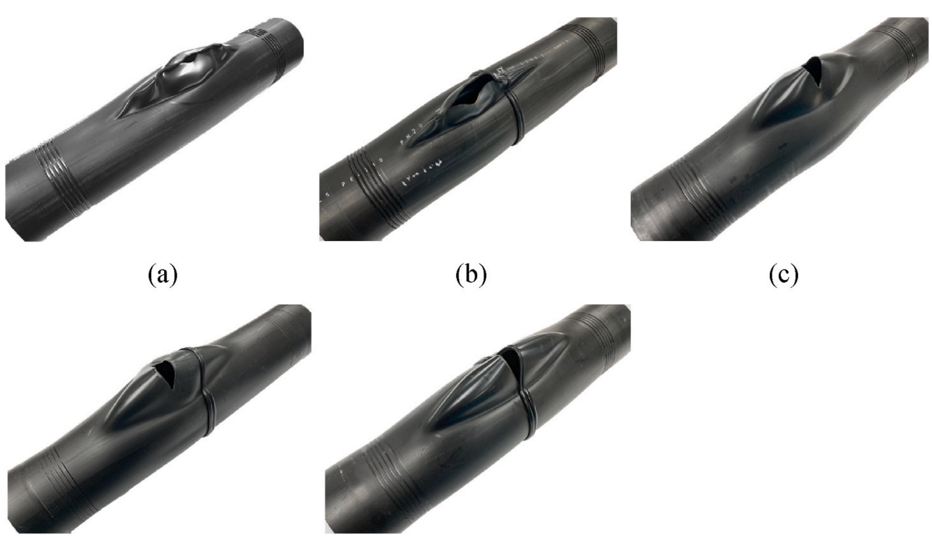

(a) (b) (c) (d) (e)

**Fig. 1.** Typical ductile failure of end-capped polyethylene pipe under quick burst internal pressure. At 23 °C (a) pipe, (b) butt fused pipe. At 80 °C, (c) pipe, (d) failure near and (e) away from the BF joint.

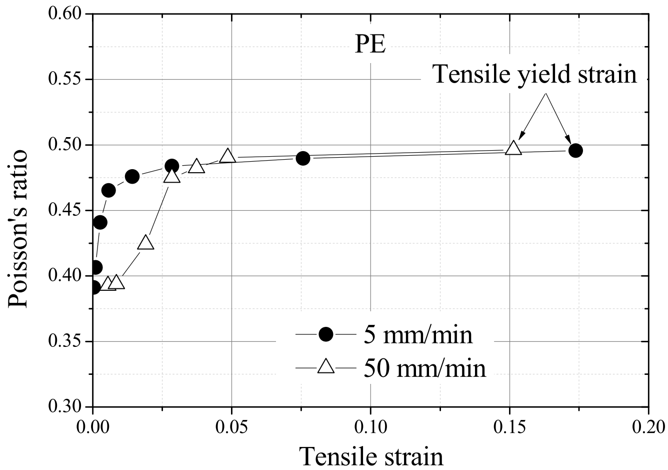


**Fig. 2.** Variation of Poisson's ratio with strain and the rate of displacement.

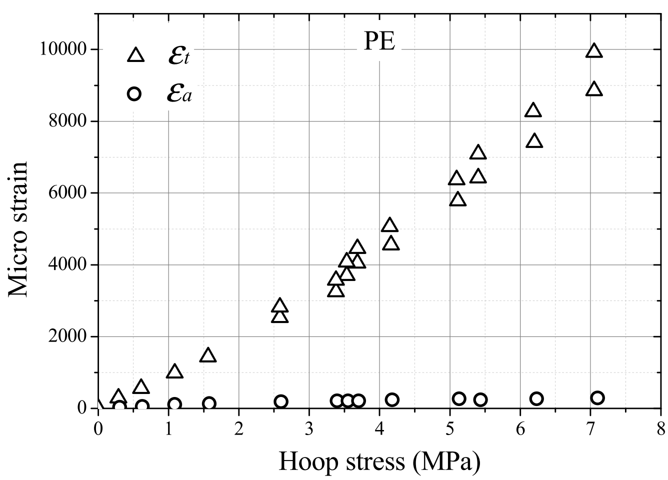


**Fig. 3.** Axial and hoop strain development in an internally pressurized 50 SDR 11 polyethylene pipe.

pipe, hoop ($\sigma_t$), axial ($\sigma_a$), and radial ($\sigma_r$) stresses develop (Eqs. (1)–(3)), and the ratio between the hoop and axial stress created at the outer surface is approximately 2:1. With the triaxial stress state developed, the yielding and cold drawing occur in the direction perpendicular to the hoop stress, which eventually induces pipe failure along the pipe axis, of the shape, depending on the temperature applied, as shown in Fig. 1.

$$\sigma_a = \frac{r_i^2 p_i}{(r_o^2 - r_i^2)} \tag{1}$$

$$\sigma_t = \frac{r_i^2 p_i}{r_o^2 - r_i^2} + \frac{(p_i) r_i^2 r_o^2}{(r_o^2 - r_i^2) r^2} \tag{2}$$

$$\sigma_r = \frac{r_i^2 p_i}{r_o^2 - r_i^2} - \frac{(p_i) r_i^2 r_o^2}{(r_o^2 - r_i^2) r^2} \tag{3}$$

Where $p_i$, $r_i$, and $r_o$, are internal pressure, inner and outer radius, respectively.

The axial strain ($\varepsilon_a$), on the other hand, becomes zero across the wall thickness when the Poisson's ratio ($\nu$) approaches 0.5, as given by Eq. (4), where $E$ is the elastic modulus.

$$\varepsilon_a = \frac{1}{E} \frac{r_i^2 p_i}{(r_o^2 - r_i^2)} (1 - 2\nu) \tag{4}$$

Fig. 2 illustrates strain and strain-dependent Poisson's ratio of pipe-grade polyethylene resin [35]. It shows the Poisson's ratio approaching a value of 0.5, far below the tensile yield strain. Fig. 3 demonstrates that while the hoop strain increases with internal pressure on 50 mm SDR 11 polyethylene pipe, the axial strain remains close to zero [35]. That is, a pipe under internal pressure, the failure cannot occur as an axial pipe fracture. However, yielding and drawing occur due to the hoop stress just before the final failure, as shown in Fig. 1.

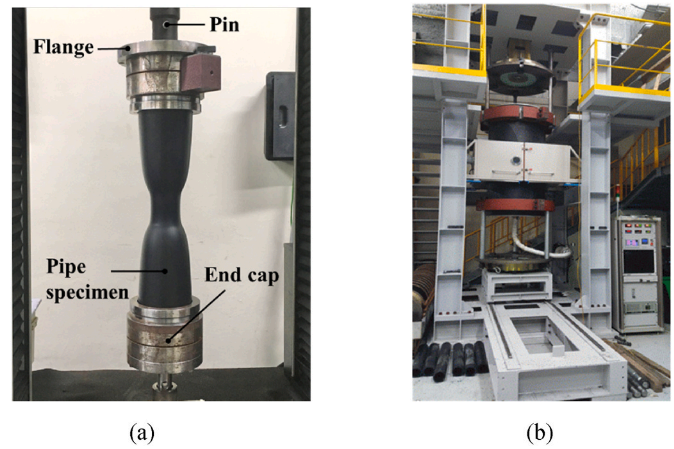


**Fig. 4.** AT test on PE-HD (a) 110 SDR 11 pipe and (b) 914 SDR 17.6 BF joint at Hannam University.

Therefore, pipe axial displacement is required to induce axial failure (perpendicular to pipe axis) in a pipe or BF joint, which is readily achieved with a whole pipe uniaxial tensile test as shown in Fig. 4. It shows a 110 SDR 11 pipe being pulled over the necking displacement and into the cold drawn region to cause large axial deformation. However, as mentioned before, performing a whole pipe axial tensile test becomes problematic as exceedingly large axial loads are required to cause deformation and failure in the pipe or BF joints as the pipe size increases (Fig. 4b).

In order to overcome the high loading requirement with the whole pipe axial tensile (AT) test, a method of using hydrostatic pressure was investigated. As discussed above, the normal hydrostatic internal pressure on an end-capped pipe produces a hoop and axial stress ratio of approximately 2:1 at the outer surface. And would cause hoop expansion with pressure while limiting the axial strain to a zero value (Fig. 3). This would imply that if the pipe is restrained from the hoop expansion, the axial tensile stress would dominate and causes axial displacement producing axial failures.

The pipe end hoop expansion restraining method reported by Wermelinger [31] and Choi [32,33] has proven to work well to determine long-term slow crack growth failures of the BF joints under sustained internal hydrostatic pressure loading. The method generated axial loading of the BF joint by mechanically preventing hoop expansion and became known as the hydro-axial tension (HAT) test. The limitation of this method is that the gap between end restraints needs to be small enough to ensure that the axial stresses developed throughout the wall thickness remain greater than the hoop stresses, as shown in Figs. 5a and 5b for inner and outer pipe surfaces, respectively [34]. As the gap displacement gets larger than about three times the BF bead width, the hoop expansion restraint tends to decrease at the inner surface of the pipe. When this happens, the hoop expansion prevails in the gap between the end restraints, as indicated by the axial and hoop stress magnitude reversal shown in Fig. 5a.

In order to overcome the shortcomings of using the hoop expansion restraining method in creating axial tension, a means of applying equal internal ($p_i$) and external pressure ($p_o$) along the end-capped pipe length was developed, as illustrated in Fig. 6. When the equal pressure ($p_i = p_o$) is applied to the inner and outer surfaces of the pipe, Eqs. (5) and (7) give axial stress (Fig. 7a), and strain (Fig. 7b) linearly increases with

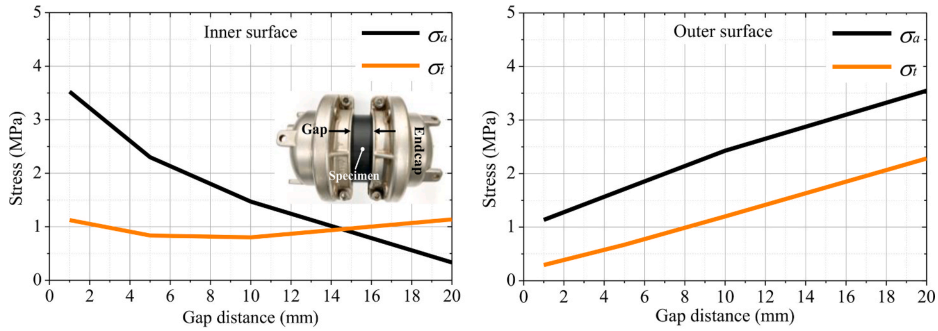


(a) (b)

**Fig. 5.** Finite element results in the hoop and axial stress variation with gap distance between end-cap restraints. (110 SDR 11 PE pipe) (a) Inner and (b) outer surface.

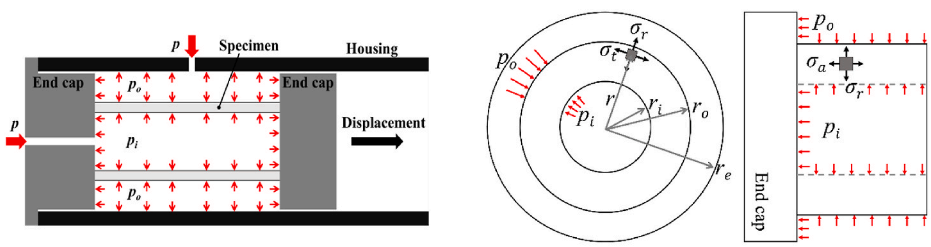


(a) (b)

**Fig. 6.** Internally pressurized end-capped pipe with equal external pressure applied along the pipe length. (a) Cross-sectional view of equal pressure loading, and (b) free-body diagram.

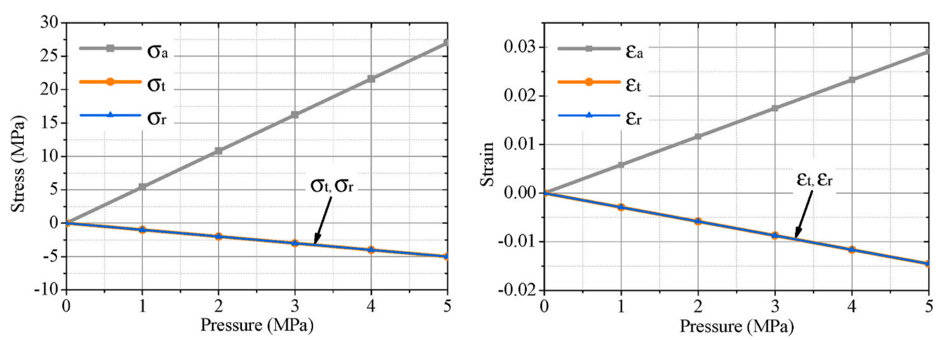


(a) (b)

**Fig. 7.** Variation of (a) stresses and (b) strains with increasing $p_i$ and $p_o$ for $p_i = p_o$ from Eqs. (5)–(8). ($r_e = 80$ mm).

increasing pressure. On the other hand, the hoop and radial stresses and strains (Eqs. (6) and (8)) tend toward larger negative values, as also shown in Figs. 7a and 7b, respectively. The tensile axial stress ($\sigma_a$) is larger than 5.4 times the compressive hoop ($\sigma_t$) and radial ($\sigma_r$) stress, and the axial strain ($\varepsilon_a$) is two times the hoop ($\varepsilon_t$) and radial ($\varepsilon_r$) strain at any applied pressure. That is, the axial stress is the maximum principle stress produced, and the axial displacement of the BF joint can be expected. It should be noted that in Fig. 6, the external pressure on the outer pipe wall portion of the end cap is included as a part of the external pressure enclosure, and this is also reflected in Eqs. (5)–(7).

For $p_i = p_o = p$

$$\varepsilon_a = \frac{p}{E}\left\{\frac{\left(r_i^2 + r_e^2 - r_o^2\right)}{\left(r_o^2 - r_i^2\right)} - 2\nu\left(\frac{r_i^2 - r_o^2}{r_o^2 - r_i^2}\right)\right\} \tag{5}$$

$$\varepsilon_t = \varepsilon_r = -\frac{p}{E}\left\{1 + \nu\left(\frac{r_e^2 - 2r_o^2 + 2r_i^2}{r_o^2 - r_i^2}\right)\right\} \tag{6}$$

$$\sigma_a = \frac{p\left(r_i^2 + r_e^2 - r_o^2\right)}{\left(r_o^2 - r_i^2\right)} \tag{7}$$

$$\sigma_t = \sigma_r = \frac{p\left(r_i^2 - r_o^2\right)}{r_o^2 - r_i^2} \tag{8}$$

The stress triaxiality ($k$) developed in the HAT can be estimated by Eq. (9) [36] and compared to the AT as follows:

$$k = \frac{\sigma_m}{\sigma_i} = \frac{\sqrt{2}\,(\sigma_1 + \sigma_2 + \sigma_3)}{3\sqrt{(\sigma_1 - \sigma_2)^2 + (\sigma_2 - \sigma_3)^2 + (\sigma_3 - \sigma_1)^2}} \tag{9}$$

Where, $\sigma_a = \sigma_1$, $\sigma_t = \sigma_2$, $\sigma_r = \sigma_3$, $\sigma_m$ = mean stress, and $\sigma_i$ = effective stress.

For HAT at $p_i = p_o = p$, $\sigma_2 = \sigma_3 = -p$, $\sigma_1 \approx 2\sigma_2 + \frac{(r_e^2 - r_o^2)p}{(r_o^2 - r_i^2)}$, and $k = 0.18$ for end cap radius $r_e$, of 80 mm. And for AT ($\sigma_1 \neq 0$, $\sigma_2 = \sigma_3 = 0$), $k =$

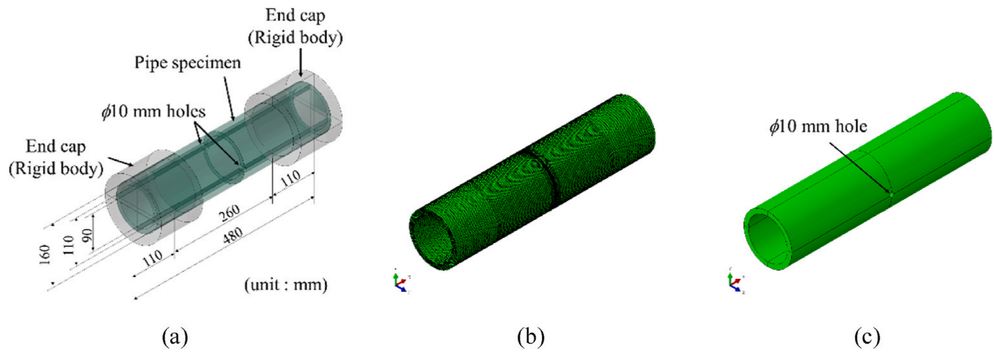


**Fig. 8.** Finite element models for HAT and AT test simulation. (a) Pipe-end cap assembly, (b) whole pipe, and (c) pipe with 10 mm diameter holes positioned at 180° apart around the pipe circumference.

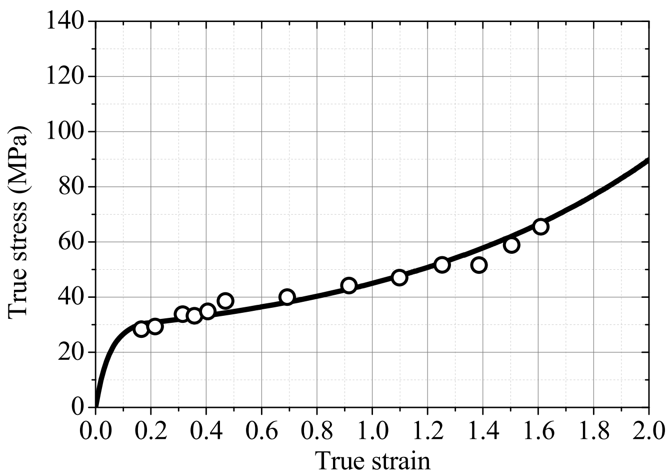


**Fig. 9.** True stress-strain curve of PE100 pipe grade resin.

0.33.

In terms of effective stress, $\sigma_{1(AT)} = \sigma_{i(AT)}$ for AT, and $\sigma_{1(HAT)} = 0.852\sigma_{i(AT)}$ for HAT. This would imply that the axial stress required to yield the pipe is about 14.8% less for HAT than the AT test.

To estimate the axial tensile response of the HAT specimen compared to the AT specimen, a finite element (FE) analysis was performed on 110 SDR 11 PE-HD pipe using ABAQUS. It is noted that the FE analysis was carried out to the point just past the onset of necking displacement. This is because the analysis was aimed to examine the axial tensile response of the whole pipe up to the onset of necking, representing the maximum force for BF joint integrity.

The finite element models for the HAT and AT specimens are shown in Fig. 8. The model consisted of a 4-node tetrahedral element (C3D4) and an 8-node linear brick element (C3D8R). The metal end caps were assumed to be rigid (R3D3 and R3D4 elements in ABAQUS). Since the end cap is almost perfectly assembled with the pipe, the analysis was performed with a TIED contact condition between them. The true stress-strain data used is shown in Fig. 9. The true stress-strain data of PE-HD were calculated from the nominal stress-strain data using Eqs. (10) and (11), respectively.

$$\boldsymbol{\sigma}_{true} = \begin{cases} \boldsymbol{\sigma}_{nom}(1+\boldsymbol{\varepsilon}_{nom}), & \boldsymbol{\sigma}_{nom} \le \boldsymbol{\sigma}_y \\ \boldsymbol{\sigma}_y\left(1+(\boldsymbol{\varepsilon}_{nom}-\boldsymbol{\varepsilon}_y)^n\right), & \boldsymbol{\sigma}_{nom} > \boldsymbol{\sigma}_y \end{cases} \tag{10}$$

$$\boldsymbol{\varepsilon}_{true} = \int_{l_0}^{l} dl \Big/ l = \ln\left(l/l_0\right) = \ln(1+\boldsymbol{\varepsilon}_{nom}) \tag{11}$$

Where, $\sigma_{nom}$, $\varepsilon_{nom}$, $\sigma_{true}$, $\varepsilon_{true}$, $\sigma_y$, $\varepsilon_y$, $n$ are the nominal stress and strain, true stress and strain, true yield stress and strain, and plastic exponent, respectively. $l_0$ is the initial gage length set at 50 mm, $l$ is the distance between gauge marks at any time $t$. An exponent value of $n = 1.25$ was chosen as this represented an optimal curve passing through the true stress and strain data points (open circle) calculated from the real-time experimental measurement of the cross-sectional area and the length change during the tensile deformation, as shown in Fig. 9.

The true stress-strain data of polymers were further converted into appropriate elastic-plastic data for FE analysis using ABAQUS. The plastic strain is obtained by subtracting the elastic strain from the total strain, as shown in Eqs. (12) and (13).

$$\varepsilon_{total} = \varepsilon_e + \varepsilon_p \tag{12}$$

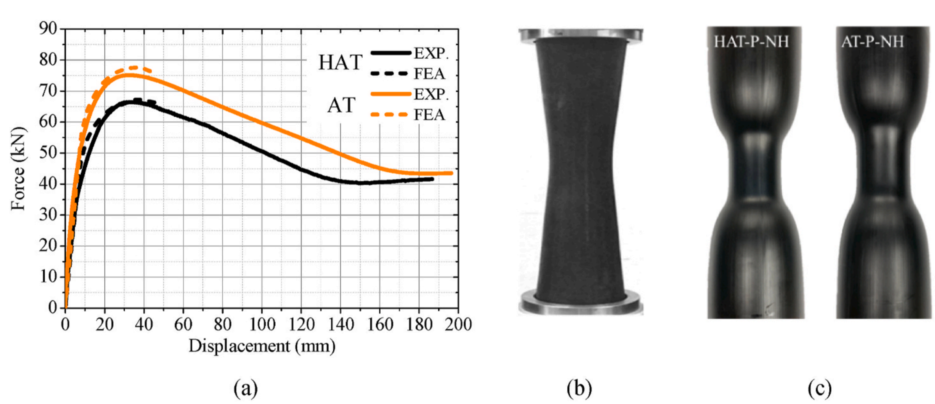


**Fig. 10.** (a) Experimental and numerical force-displacement curves of HAT-P and AT-P test. (b) AT-P specimen showing diffused necking at 80 mm displacement, and (b) HAT and AT specimens undergone cold drawing shortly after full necking.

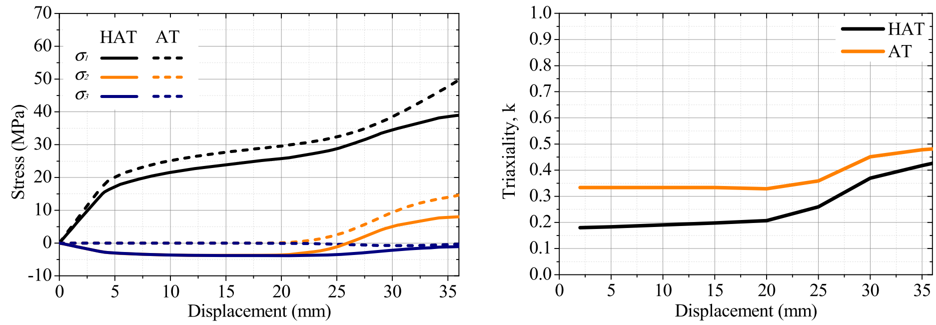


(a) (b)

**Fig. 11.** (a) Principle stresses and (b) stress triaxiality with end cap displacement at the pipe center from FE analysis.

$$\varepsilon_p = \ln(1+\varepsilon_{nom}) - \ln(1+\sigma_y / E), \ \varepsilon_{nom} \geq \varepsilon_y \tag{13}$$

Where $\varepsilon_{total}$, $\varepsilon_e$, $\varepsilon_p$ and $E$ are true total strain, true elastic strain, true plastic strain, and tensile modulus, respectively. The independent elastic constants ($E = 1.1$ GPa, $\sigma_y = 18.5$ MPa, $\varepsilon_y = 0.03037$, $\nu = 0.45$) were used to describe the elastic part. The plastic part after the yield strength was tabulated from the fitted true stress-strain curve.

### 2.2. Analysis of HAT whole pipe test (HAT-P)

The force-displacement curves of HAT-P and AT-P specimens obtained from FE analysis and experiment are shown in Fig. 10a. The whole pipe appearance during diffused necking and after undergoing full neck formation during AT test is illustrated in Fig. 10b. The experimental and numerical force-displacement behavior between HAT and AT up to the point of onset of necking is similar in shape. The difference in maximum force is also similar in magnitude, 12.6% experimental versus 13.4% numerical. This difference in terms of the pipe axial stress, $\sigma_1$, at the center of the pipe, translates to about a 13% difference (Fig. 11a). And this is similar to the value (14.8%) calculated between HAT (triaxiality, $k = 0.18$) and AT ($k = 0.33$) specimens, as previously mentioned above (Eq. (9)).

Fig. 11a shows FE analysis results on the stresses developed at the center of the necking instability. $\sigma_1$ in HAT and AT is always maintained as the maximum principal stress, increasing with the pipe axial displacement. On the other hand, with the HAT, the hoop $\sigma_2$ and radial $\sigma_3$ stresses maintained negative values up to the point of yielding (~20 mm displacement). Then both stresses tend toward positive values with increasing displacement (Fig. 11a). The rate of $\sigma_2$ increase is higher than $\sigma_3$, approaching a zero value at 25 mm and increase toward the positive magnitude. $\sigma_3$, on the other hand, approaches zero at a displacement of about 35 mm (onset of necking) and maintains zero upon further displacement. In AT, the hoop $\sigma_2$ and radial $\sigma_3$ stresses were initially zero, and at the point of yielding, positive $\sigma_2$ develops and increases similar to HAT (Fig. 11a). $\sigma_3$ in AT is kept zero throughout pipe axial displacement, while $\sigma_3$ in HAT also reaches zero at the point of onset of necking. The stress behavior in terms of the stress triaxiality is illustrated in Fig. 11b. The stress triaxiality in both HAT ($k = 0.18$) and AT ($k = 0.33$) is somewhat maintained up to the point of yielding (~20 mm displacement), and then both tend to increase toward higher values. At the onset of necking, the stress triaxiality for HAT and AT becomes 0.43 and 0.48, respectively. These values indicate similar biaxial tension developing ($\sigma_1$ and $\sigma_2$) in HAT and AT specimens during yielding and necking, with pipe axial stress ($\sigma_1$) being the dominating maximum principal stress. Therefore, although HAT ($k = 0.18$ to 0.43) and AT ($k = 0.33$ to 0.48) exhibit different stress triaxiality values up to the onset of necking, HAT creates pipe axial stress, $\sigma_1$, as the maximum principal stress and hence lends itself to be a unique tensile test for evaluating the whole pipe under axial tension. In addition, the tensile force required to cause necking is less with the HAT (Fig. 10a), it is a more conservative test than the AT test. Furthermore, when comparing the tensile characteristics, for example, of whole pipe BF joints, HAT is also a viable tensile test, with a significant advantage of using normal pipe internal pressure testing equipment, which is readily available in pipe testing laboratories.

### 2.3. Analysis of HAT whole pipe test of a specimen with center holes (HAT-P-WH)

In terms of the practicality of performing the HAT test on pipe BF joint, the equal pressure ($p_i = p_o$) can be more easily achieved by introducing small diameter holes made in the pipe at the BF joint location. These holes are used to deliver and equalize the internally applied pressure to the outer surface of the pipe (Fig. 12), rather than applying $p_i$ and $p_o$ separately (Fig. 6a). Holes at the BF joint location also help concentrate the stress on the joint to facilitate joint failures. The diameter of the hole is 10 mm, and this is the same notch tip diameter used in the coupon test of notched fusion zone tensile (NFZT) [37] and waisted tensile (WTT) [18] specimens for testing BF joints. To maintain symmetry, the two holes are made 180° apart around the pipe

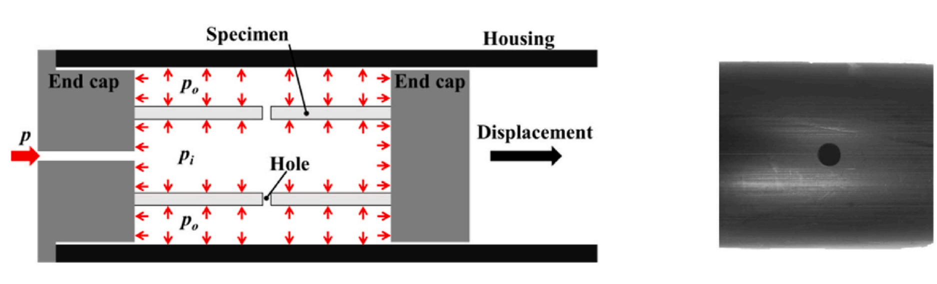


(a) (b)

**Fig. 12.** (a) Illustration of HAT-P-WH test, and (b) the holes made at 180° apart in the pipe center.

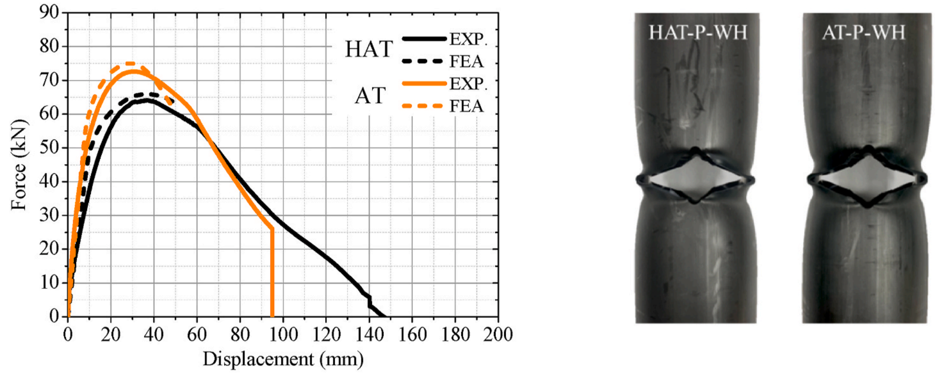


(a)　(b)

**Fig. 13.** HAT-P-WH and AT-P-WH test. (a) Experimental and numerical force-displacement curves and (b) specimen appearance at cold drawing shortly after full necking.

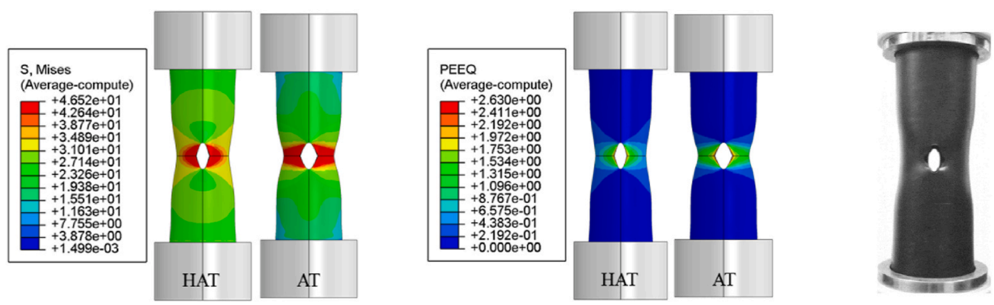


(a)　(b)　(c)

**Fig. 14.** FEA results for AT and HAT containing holes at 40 mm pipe axial displacements. (a) von-Mises stress, and (b) equivalent plastic strain contours. (c) AT test at 40 mm displacement.

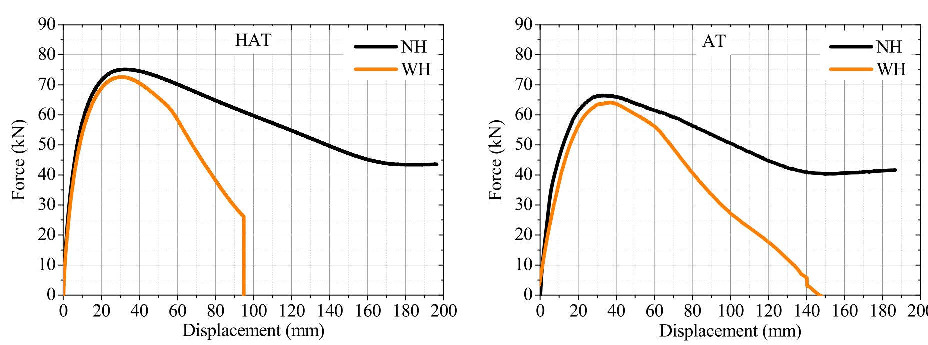


(a)　(b)

**Fig. 15.** Comparison of experimental force-displacement curve. (a) HAT and (b) AT test with holes and no hole.

circumference. The FE model of the whole pipe with two holes on the pipe center is shown in Fig. 9c, with the same model elements as before.

The results from the FE analysis are shown in Fig. 13, along with the experimental HAT and AT tested data. The experimental and numerical force-displacement behavior between HAT and AT test is similar in shape up to the onset of necking, as shown in Fig. 13a. The difference in maximum applied force between HAT and AT is also similar in magnitude, where HAT values are lower by 11.7% experimental versus 12.4% numerical. The computed shape of HAT and AT specimen at 40 mm axial displacement is also similar to the experimental AT specimen at a similar displacement shown in Fig. 14. The von-Mises stress (Fig. 14a) and plastic strain (Fig. 14b) contours indicate, while the higher stress and strain concentration is localized to the hole area of the pipe in HAT, these extend from the hole and cover the total pipe circumference in AT as shown. Hence, the axial force is expected to decrease more rapidly in AT than with HAT, as shown in Fig. 13a.

The failure appearances are also similar between HAT and AT (Fig. 13b) in that the elongated hole in the neck (Fig. 14c) underwent tearing as indicated by the rapid force drop after reaching the maximum force in both AT and HAT test, compared to the necking in no hole specimens (Fig. 10a). The tear growth was in the direction perpendicular to the pipe axis in both specimens, induced by the higher stress at the hole, as shown in Fig. 14a.

**Table 1**
Mean maximum force and standard deviation of HAT-P and AT-P tests.

| Test | Maximum force (N) | |
|---|---|---|
| | NH | WH |
| HAT | 66,509 ± 496 | 63,870 ± 662 |
| AT | 74,472 ± 783 | 73,132 ± 461 |

(a) (b)

**Fig. 16.** Preparation of FPC joint. (a) Before and (b) after applying fine quicklime particulates.

## 2.4. Comparison between HAT-P-NH and HAT-P-WH

Fig. 15 and Table 1 illustrate the comparison between pipe specimens with and without holes. Both HAT-P-WH and AT-P-WH show that the force-displacement curve is slightly lower than P–NH specimens and exhibits faster force drop starting from the maximum force. These results are due to the hole tearing versus pipe necking after reaching the maximum force. The standard deviation of the maximum force of each test is within ±2%, indicating good reproducibility of the tests. The experimental and numerical results suggest that depending on what one is trying to obtain from the pipe axial tensile testing, either pipe with holes or no hole can be utilized. It will be shown that in assessing the structural integrity of the whole pipe BF joint, a pipe BF containing holes provides better characterization of the defect present in the fusion joint and provides better pressure delivery control during testing.

# 3. Experimental

## 3.1. Material

Samples were received as extruded PE100 110 SDR 11 black pipes from a local supplier, and they were cut to dimensions and butt fused to provide various joint integrity. AT and HAT specimens were all made from these pipes. The tensile yield stress, fracture strain, and modulus of elasticity were 25 MPa, > 600%, and 1.1 GPa, as measured by the ISO 527–2. The density of the polyethylene resin and the melt flow rate were 960 kg/m$^3$ (ISO 1183–12, Method 1) and 0.25 g/10 min (ISO 1133), respectively.

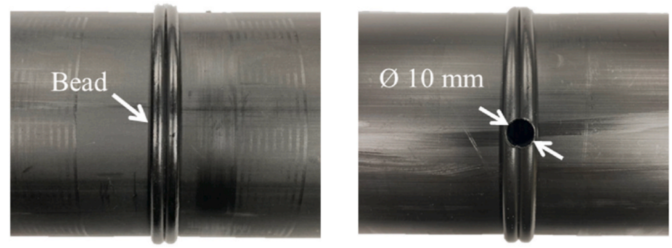


(a) (b)

**Fig. 18.** BF–NI specimen with (a) no hole and (b) with holes on the bead.

## 3.2. Method

### 3.2.1. Pipe specimen

Pipe specimens for AT and HAT tests were made to a total length of 460 mm. They were conditions at 23 °C for at least 24 h prior to the test.

### 3.2.2. Butt fused specimen

Three types of BF joints, a normal joint with no flaw (NI), a cold fusion (CF) joint, and a joint with fine particulate contamination (FPC), were made. All joints were made using two 250 mm long pipes in a Georg Fischer TD-315 BF machine according to the SLP procedure of ISO 21307. The heating plate temperature was 230 °C, and the jointing pressure of 1.5 bar was applied for all butt-fusions. CF joints were produced by increasing the change over time (COT) of the pressure-time BF curve (ISO 21307). A normal 5 s COT was used to create NI and FPC joints, while a COT of 70 s was employed to produce the CF joint. A 70-s COT was found to be adequate to have the heated interface of 110 SDR 11 pipe to cool down to nearly the crystallization temperature of the pipe resin, resulting in cold fusion in the BF joint [38]. All jointing was done at an ambient temperature of 23 °C, 50% relative humidity. The BF joint with FPC was made using fine quicklime particulates. After planar machining to square each pipe ends, quicklime particles were applied to each end using a soft cloth glove until a predetermined amount of fine particulates covered the total pipe end surfaces (Fig. 16). The SLP BF procedure was then applied with 5 s COT. Fig. 17 illustrates the relative bead shape and size of NI, CF, and FPC BF joints. For FPC, the squeeze melt flow during BF jointing causes much of the fine particulates to flow out and accumulate on the surface of the fusion bead, as shown in Fig. 17b. On the other hand, CF causes the bead shape and size to be different from the normal NI joint (Fig. 17a). For some BF joints, two 10 mm diameter holes were drilled completely through the BF at 180° apart along the circumference, as shown in Fig. 18. BF pipes were left at ambient conditions for 24 h before final dimensioning using a lathe to a total length of 460 mm for both the AT and HAT tests. All specimens were then conditioned at 23 °C, 50% RH for at least 24 h before the test.

## 3.3. Test jigs for HAT and AT tests

Test jigs for AT and HAT tests were designed to hold the axial load

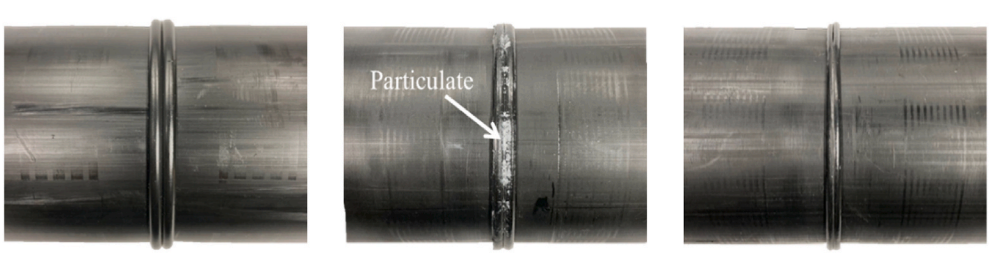


(a) (b) (c)

**Fig. 17.** Relative shape and size of BF bead. (a) NI, (b) FPC, and (c) CF joint.

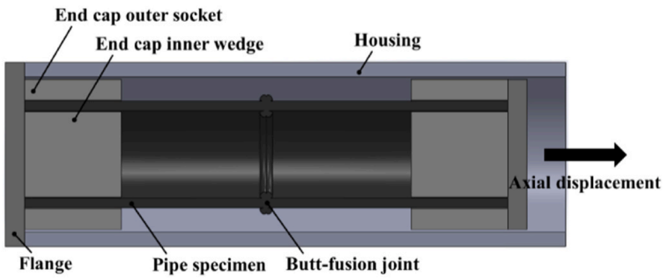


**Fig. 19.** Illustration of a HAT test jig assembly.

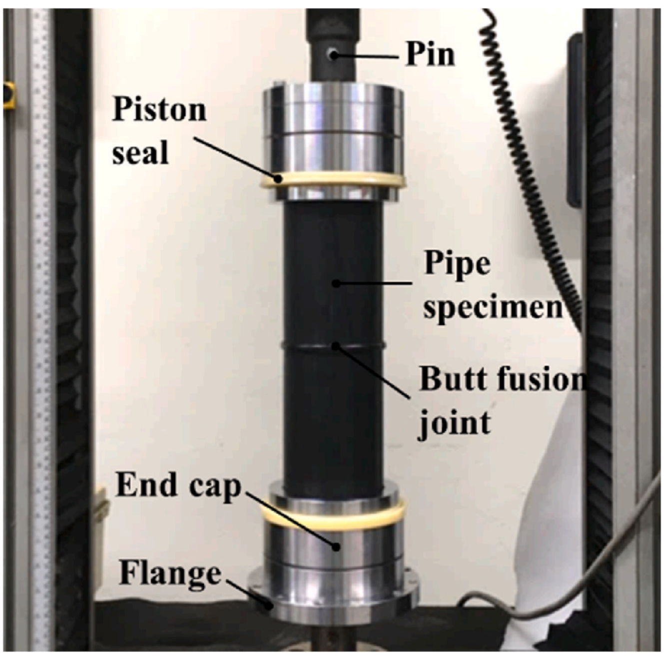


**Fig. 20.** Set up for AT-BF test.

through the pipe inner and outer pipe surfaces. The HAT test jig is also made to hold the internal and external pressures along the pipe length. The axial pipe loading in AT test was achieved through the end cap assembly fitted at both pipe ends (Fig. 19). The assembly consisted of an internal wedge for the inner pipe wall and an end cap for the outer pipe wall. The load is applied through the internal wedge, and the end cap on the outer wall would allow further tightening of the pipe ends with pipe axial displacement and hold the increasing axial load. In the HAT test, the same end cap assembly was used in addition to an outer steel housing with which the external pressure is accommodated through movable seals on both end caps (Fig. 19). In this case, one end cap was fixed to the outer housing by a flange, while the other end cap was free to extend axially along the inner wall of the housing with the pressure increase. The internal pressure applied pushes the internal wedge and causes axial displacement of the pipe (Fig. 19).

In one design, the hydrostatic pressure is supplied directly to the pipe inside by a single inlet, and the pressure entering fills the outer pipe wall with equal pressure through the holes made in the BF joint (Figs. 12a and 18b). In another design, two pressure inlets in a single manifold were employed to directly apply the same internal and external pressures (Fig. 6a). In this case, no hole was made on the BF joint.

### 3.4. HAT and AT tests

Pipe specimens with no BF joint, NI, FPC, and CF BF joints were AT and HAT tested. Both specimens with and without holes were used. Each

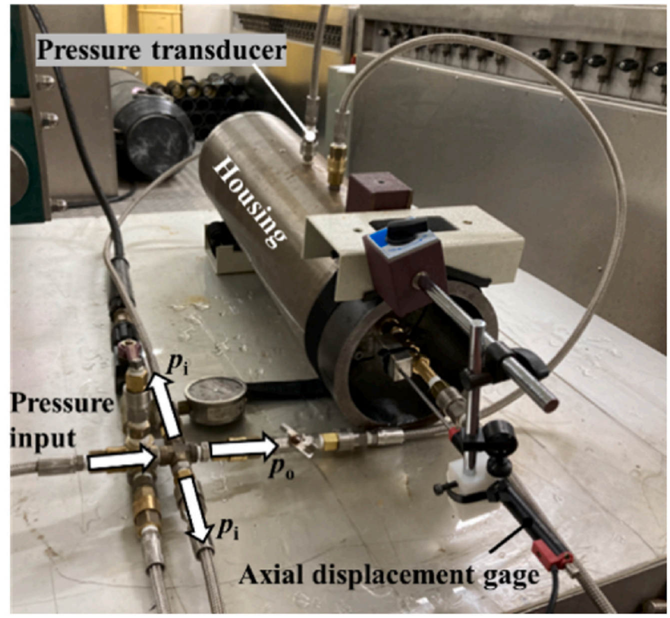


**Fig. 21.** Set up for HAT test.

AT and HAT test was repeated at least five times, and all tests were carried out at 23 °C, 50% relative humidity environment.

#### 3.4.1. AT test

The AT test was carried out on a universal testing machine (Instron Deutschland GmbH, 4482) with a 100 kN load cell. The AT specimen fitted with end cap assembly was placed on the testing machine using universal joints, as shown in Figs. 4a and 20. The tensile test was performed using the cross-head speed of 50 mm/min. The force-displacement curves up to the complete BF failure or the gross yielding of the specimen were recorded. The cross-head displacement measured the pipe displacement, and after each test, the energy value to failure was determined from the force-displacement curve.

#### 3.4.2. HAT test

The pipe specimen assembly was inserted into the outer steel housing after fitting the pipe ends with the outer end cap-internal wedge assembly. The inner surface of the housing guides the end caps' piston seal that is allowed to move with minimum friction when internal and external pressures are applied. Both inner pipe and outer pipe walls were then filled with tap water through an inlet fitting at the outer steel housing shown in Fig. 21. The pressure was then increased at a 120 bar/min rate using a pump that delivered up to 80 bar maximum pressure. Water temperature was maintained at 23 °C throughout the test. The pressure and the pipe end displacement were measured using a pressure gage (TIVAL SENSORS GmbH, TST-10.0) located at the outlet fitting in the housing and an LVDT placed at the moving end cap, respectively. The data from each sensor were simultaneously collected by a data acquisition system (GRAPHTEC Corporation, GL820) at a rate of 10 Hz. After each test, the pressure-displacement data was converted to a force-displacement curve that determined the energy value to failure.

#### 3.4.3. Fracture surface examination

The fracture surfaces of the failed BF joints containing FPC and CF flaws were observed under the scanning electron microscope (SEM). The samples for the SEM examination were first cut from the BF area containing the full thickness of the pipe wall and the BF beads. The cut specimens were then Pt coated in a sputtering machine (Agar Scientific Ltd., AGB7341) and observed under SEM (Jeol Ltd., JSM-7610F Plus) using an accelerated potential of 25 kV. EDX measurement on a fracture surface containing fine particulate was also done to confirm the presence

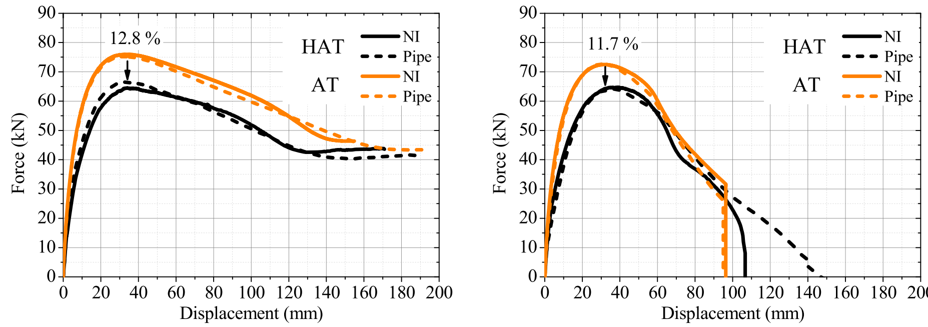


(a) (b)

**Fig. 22.** HAT and AT results for pipe and NI joint. (a) NH and (b) WH.

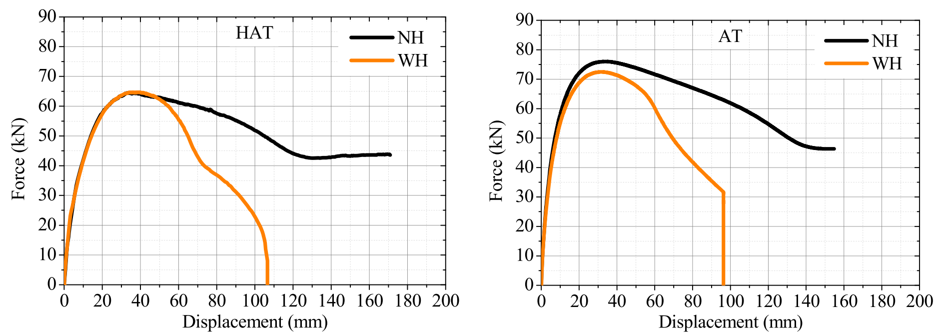


(a) (b)

**Fig. 23.** Comparison of experimental force-displacement behavior of NI–NH and NI-WH joint. (a) HAT and (b) AT test.

of the fine quicklime particulate.

## 4. Results and discussion

HAT and AT tests results from the whole pipe and whole pipe with BF joints are compared. Both normal (NI) and flawed (CF and FPC) BF joint behavior is described, and BF joint having no hole (NH) and with holes (WH) are presented.

### 4.1. Whole pipe and BF–NI joint

Fig. 22 illustrates the HAT and AT test results from the whole pipe and whole pipe with BF–NI joint. For each specimen type (Pipe, BF, NH, and WH), the shape of the force-displacement curve is similar in both HAT and AT tests. And the maximum force is lower by 12.8% (for NH specimen) and 11.7% (for WH specimen), between the HAT and AT test, as shown. The similarity in the force-displacement curve between the pipe and BF specimens is due to both specimens undergoing yielding, necking, and cold drawing in the pipe region (Figs. 10c, 24b and 25b) for NH specimens. With WH specimens, the similarity comes from tear initiating from the hole and tear propagating along the pipe circumference, perpendicular to the pipe axis, after the onset of necking (Figs. 13b, 29b and 30b).

### 4.2. NH and WH BF–NI joints

Fig. 23 shows the force-displacement curves between the NI–NH and NI-WH joints tested under HAT (Fig. 23a) and AT (Fig. 23b). There is practically no difference in the force-displacement curve between the NH and WH joints up to the point of onset of necking (maximum force) for the HAT test and a small difference (>5%) observed for AT test. These results are very similar to the comparison made between the

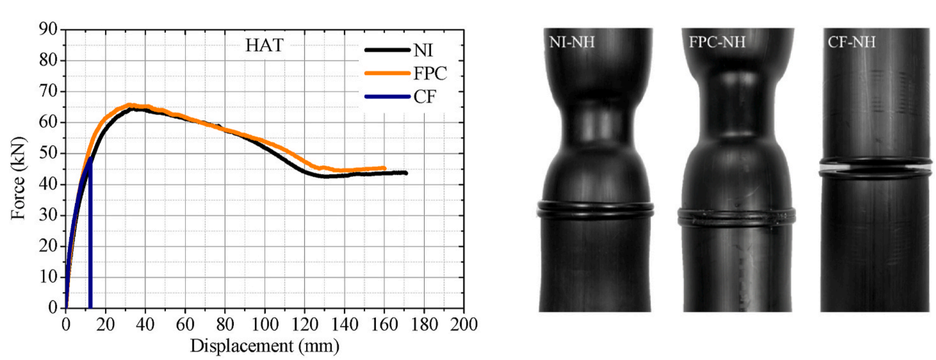


(a) (b)

**Fig. 24.** HAT test on flawed BF joint with no holes. (a) Force-displacement curves, and (b) specimens after the test.

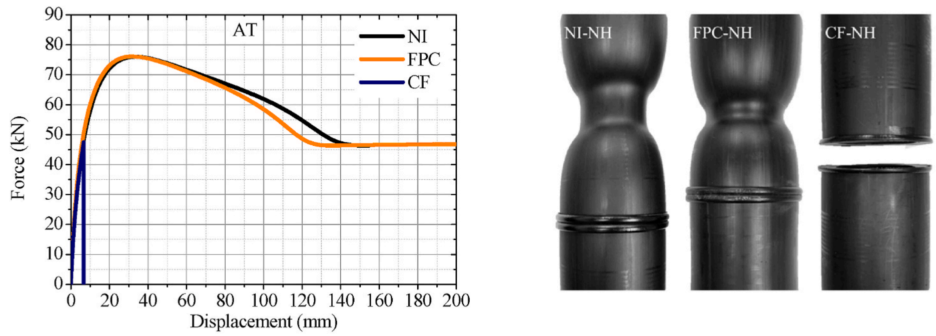


(a) (b)

**Fig. 25.** AT test on flawed BF joint with no holes. (a) Force-displacement curves, and (b) specimens after the test.

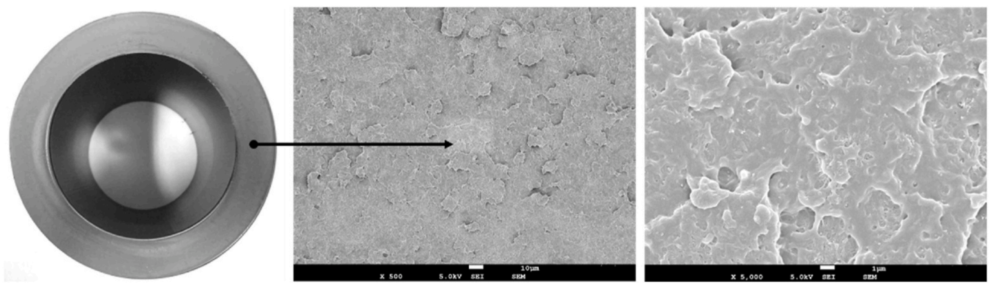

(a) (b) (c)

**Fig. 26.** Fracture surface of CF specimen after HAT test. (a) Pipe cross-section, (b) ×500 and (c) x5000.

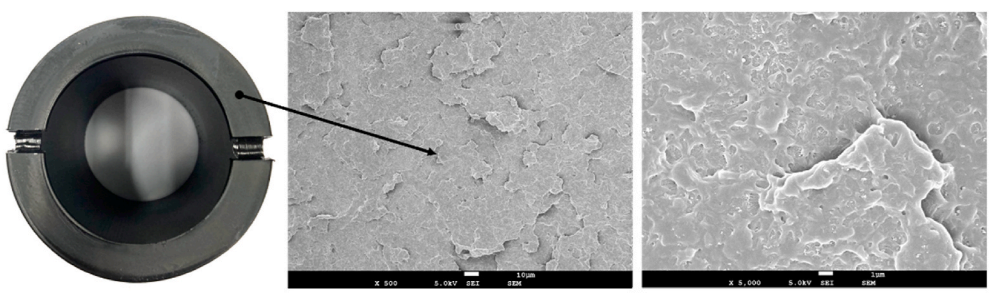

(a) (b) (c)

**Fig. 27.** Fracture surface of CF specimen after AT test. (a) Pipe cross-section, (b) ×500 and (c) x5000.

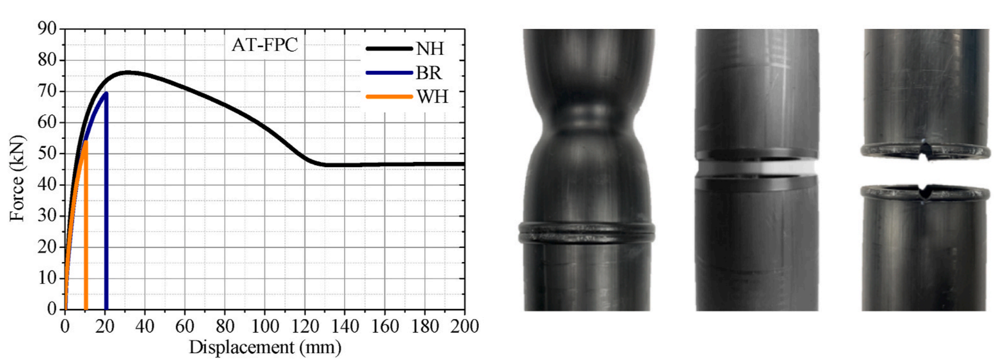


(a) (b) (c) (d)

**Fig. 28.** AT tests on FPC specimens with different bead types. (a) Force-displacement curves, (b) bead intact, (c) bead removed, and (d) bead with holes (WH).

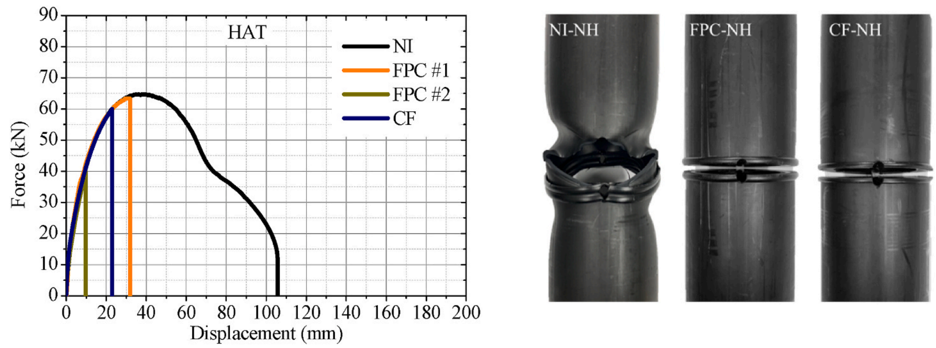


(a) (b)

**Fig. 29.** (a) Force-displacement curves of HAT tests with holes, and (b) specimens after HAT test.

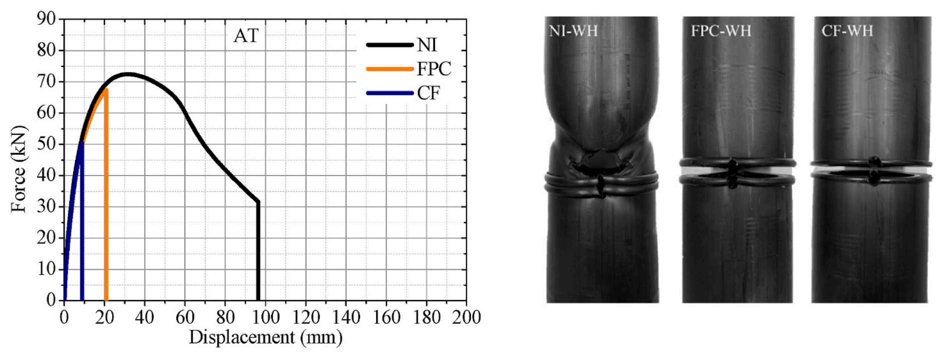


(a) (b)

**Fig. 30.** (a) Force-displacement curves of AT tests with holes, and (b) specimens after AT test.

whole pipe WH and NH specimens, as previously demonstrated in Fig. 15. As indicated above, with NH specimen, yielding, necking, and cold drawing occurred in the pipe region away from the BF joint (Figs. 24b and 25b). This can be attributed to the BF joint having a larger cross-sectional area (by about 50% more for 110 SDR 11 pipe) than the adjacent pipe due to the additional area produced as a result of the BF bead. Thus, the post-yield deformation is expected in the pipe region, as observed. With WH specimen, after the onset of necking displacement, hole tear initiates and propagates along the circumference of the pipe just adjacent to the BF bead (Figs. 29b and 30b). The ductile tear failure observed in BF joints adjacent to the bead is due to the high-stress concentration caused by the sharp contact produced between the beadroll and the pipe outer wall [39].

### 4.3. Flawed (CF and FPC) BF–NH joint

The results of HAT and AT tests on FPC-NH and CF-NH joints are given in Figs. 24 and 25, respectively, with the result from the NI–NH joint. All CF-NH joints failed in a brittle manner (separation at the joint interface), as shown by the force-displacement curves (Figs. 24a and 25a). The failure appearances (Figs. 24b and 25b) are also identical, independent of the type of test, and almost no deformation can be seen in the failed CF joint specimens. Figs. 26 and 27 show the fracture surfaces joints in detail from the HAT (CF–NH) and AT (CF-WH) tests, respectively. They are seen to have identical fracture surface features. What seems to be smooth flat fracture surfaces (Figs. 26a and 27a) show a high concentration of uniformly distributed "scales" at ×500 magnification (Figs. 26b and 27b). At still higher magnification (×5000), minimum micro-ductility "scale fractures" (Figs. 26c and 27c) are shown, indicative of the observed brittle fracture of the CF joints.

Unlike the CF-NH joint, the FPC-NH joint did not undergo brittle fracture, as shown in Figs. 24 and 25. A force-displacement behavior similar to that of the NI–NH joint in HAT and AT tests was observed. This is speculated to be caused by two effects. One is due to much of the FPC being squeezed out from the joint interface to the BF bead during fusion jointing (Fig. 17b). The other is caused by the reduced stress in the joint compared to the adjacent pipe due to the increased cross-sectional area of the BF joint area by about 50%, produced by the BF bead. Therefore, although FPC containing BF joints are known flaws in the joint, it was shown to withstand the maximum force and to cause adjacent pipe area to undergo necking, as indicated in Figs. 24b and 25b.

To better understand the cause for FPC-NH joint behavior, the outer BF bead of the FPC joint was removed and AT tested. This would effectively reduce the joint cross-section area by about 25%. The result is shown in Fig. 28. The force-displacement curve (Fig. 28a) and the fracture appearance (Fig. 28c) clearly indicate brittle failure of the joint, similar to that observed with the CF joint mentioned above. Therefore, the FPC joint strengthened by the additional BF bead cross-sectional area was the cause for the FPC joint behavior observed in Figs. 24 and 25.

Another way of creating a brittle fracture in the FPC joint is using holes in the joint, as shown in Fig. 18b. This would impose a stress concentration (Fig. 14) on the FPC joint hole area while reducing the cross-sectional area by about 6.5%. The AT test result on FPC-WH is given in Fig. 28. Brittle failure again occurred in the FPC-WH joint (Fig. 28d), similar to the outer bead removed FPC specimen (Fig. 28c).

Therefore, it is advantageous to make use of the hole in the joint, as the stress concentration created in the hole and cross-sectional area reduction effect can potentially pick out the flawed BF joints. In terms of experimental practicality, HAT with-hole specimen is preferred to the outer bead removed specimen. Since an ovality often exists in the pipe cross-section, removing joint bead uniformly is not always easy.

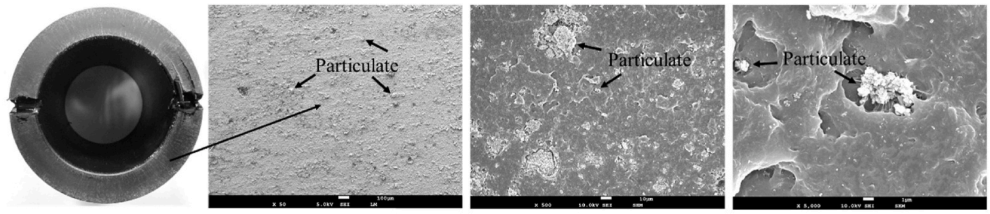


(a) (b) (c) (d)

**Fig. 31.** Fracture surface of HAT tested FPC joint. (a) Pipe cross-section, (b) x50, (c) ×500 and (d) x5000.

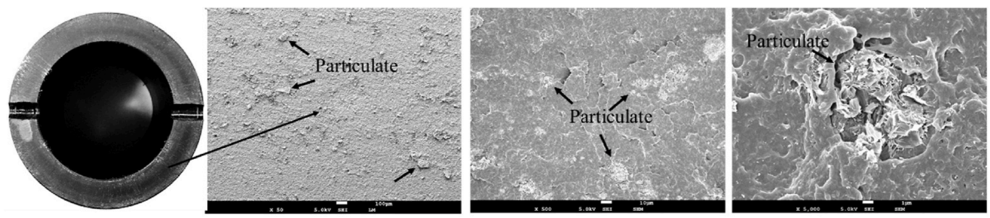


(a) (b) (c) (d)

**Fig. 32.** Fracture surface of AT tested FPC joint. (a) pipe cross-section, (b) x50, (c) ×500 and (d) x5000.

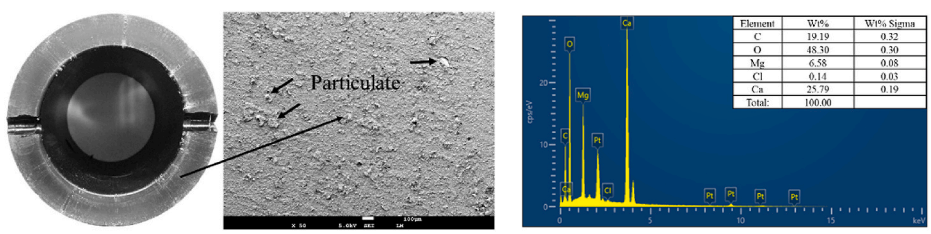


(a) (b) (c)

**Fig. 33.** HAT tested FPC joint with higher FPC concentration. (a) pipe cross-section, (b) fracture surface at x50, and (c) SEM-EDX spectrum of quicklime particulate.

Whereas introducing two holes on BF bead can be readily done by simple drilling. Also, as compared to the BF–NH joint, the BF-WH joint specimen provides better control of the equal external and internal pressures required during the HAT test (Fig. 6a versus Fig. 12a). Finally, the 10 mm diameter hole used is the same notch diameter as the ISO 13954 coupon test specimen for the BF joint. The purpose of the notch is the same, for creating stress concentration to facilitate flaw joint failures.

### 4.4. Flawed (CF and FPC) BF-WH joint

The results of HAT and AT tests on FPC-WH and CF-WH joints are given in Figs. 29 and 30 , respectively, with the result from the NI-WH joint. All CF joints failed in a brittle manner, as indicated by the force-displacement curve (Figs. 29a and 30a) and the failure appearance (Figs. 29b and 30b). As with the CF-NH joint, almost no deformation can be seen in the failed CF-WH joint. Same "scale fracture" features (Figs. 26 and 27) were also seen on fractured CF-WH joints.

Similarly, brittle fractures also occurred in FPC-WH joints under both HAT and AT tests (Figs. 29 and 30), and they were very similar to CF joint fractures. The fracture surface details are shown in Figs. 31 and 32. The distribution of fine particulate contaminants is seen on joint fracture surfaces (Figs. 31b and 32b). At ×500 magnification, FPC is seen to be embedded on the surfaces surrounded by similar "scale fractures" (Figs. 31c and 32c). These scale fracture fractures seem to be tunneled deeper into the joint surface (Figs. 31d and 32d) than the CF scale fractures (Figs. 26c and 27c), indicating higher interfacial temperature at the time of fusion jointing. The ductility is seen to be at its minimum and hence observed brittle fracture of the FPC joint. The FPC was

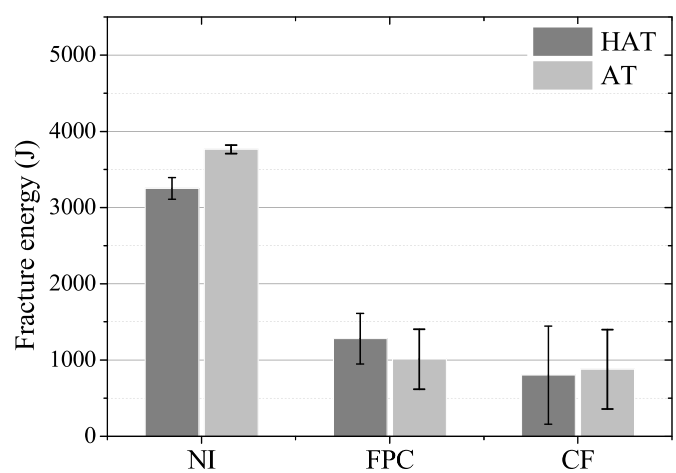


**Fig. 34.** Fracture energies of various BF joints from HAT and AT tests with holes.

confirmed to be the remaining quicklime applied during BF jointing, as observed by the SEM-EDX spectrum shown in Fig. 33c.

Figs. 31 and 33 are the HAT FPC fracture surfaces of lower (FPC#1) and higher (FPC#2) levels of FPC concentration, respectively. The corresponding force-displacement curves in Fig. 29 show that the FPC joint with a higher FPC level fractured at smaller displacement than the lower level. Hence, the HAT test can also differentiate the force-displacement

**Table 2**
Fracture energies determined from HAT and AT tests on specimens with holes.

| Joint type | Fracture energy [J] | |
|---|---|---|
| | HAT | AT |
| NI | 3252 ± 142 | 3764 ± 57 |
| FPC | 1281 ± 332 | 1012 ± 393 |
| CF | 802 ± 598 | 877 ± 520 |

behavior between the levels of FPC concentrations.

Fig. 34 and Table 2 illustrate the fracture energies determined from the force-displacement curves for each type of BF-WH joint, using both HAT and AT tests. The fracture energies were taken directly from the area under the force-displacement curve for FPC and CF joints. The area under the curve up to 70 mm displacement was used for the NI joint, as this approximates the onset of full necking displacement. The fracture energies indicate the value of the HAT test for correctly and reproducibly depicting the fracture behavior of different types of BF joints. High fracture energies were found for NI, and significantly reduced (>70%) fracture energies were indicative of the FPC and CF flawed joints. The higher standard deviation found for FPC and CF joints than the NI joint is due to the difficulty of making FPC and CF joints and not the test method themselves.

## 5. Conclusions

In this work, a whole pipe axial tensile test using hydrostatic pressure was developed and successfully used to evaluate the integrity of polyethylene whole pipe BF joints having various types of flaws. The hydro-axial tension (HAT) test developed utilizes equal internal and external pressures on the pipe to minimize hoop and radial stresses while allowing axial stress to be the dominant principal stress driving the axial tensile displacement. The finite element analysis has shown that the stress triaxiality developed in the HAT ($k = 0.18$) test is different from the whole pipe axial tensile (AT) test ($k = 0.33$) initially and approaches $k = 0.43$ for HAT and $k = 0.48$ for AT test at the onset of necking displacement. This in terms of the maximum tensile force required to cause the onset of necking, translates to HAT having a lower force requirement by about 13% compared to the AT test, as experimentally confirmed. Hence, in itself, the HAT test is considered a unique tensile test for evaluating the whole pipe under axial tension force. The force-displacement behavior and the failure appearance were experimentally and numerically found to be similar between HAT and AT specimens, both with holes and without holes on the pipe and BF joints. The application of the HAT test to evaluate BF joints containing various types of flaws was investigated. It correctly and reproducibly depicted flawed joints (CF and FPC) and joints with no imperfections (NI), as with AT test. In comparing the BF fracture energies of various BF joints, HAT and AT tests showed the same trend with fracture energy reduction greater than 70% with CF and FPC containing BF joints as compared to the NI joint. The fracture surface features were identified for CF and FPC joints, and a concentrated "scale fracture" with minimized ductility was determined to be the cause for brittle fractures. The HAT and AT specimens with holes in the BF joint were shown to be the best at evaluating the BF joint integrity, particularly for identifying FPC joints. The HAT test also demonstrated its capability to differentiate joints with differing FPC levels. In terms of practicality in performing the HAT test, the specimen with holes is the preferred way of readily applying equal internal and external pressure to the pipe.

## Declaration of competing interest

The authors declare that they have no known competing financial interests or personal relationships that could have appeared to influence the work reported in this paper.


## Acknowledgment

The authors acknowledge the financial support provided by the Nuclear Power Core Technology Development Program of the Korea Institute of Energy Technology Evaluation and Planning (KETEP), Ministry of Trade, Industry & Energy, Republic of Korea (Project no. 20181520102810).


## References


[1] J. Shi, A. Hu, F. Yu, Y. Cui, R. Yang, J. Zheng, Finite element analysis of high-density polyethylene pipe in pipe gallery of nuclear power plants, Nucl. Eng. Technol. 53 (2021) 1004–1012.
[2] G. Tsakiris, V. Tsakiris, Pipe Technologies for Urban Water Conveyance Distribution Systems, Water Util. J., 2012, pp. 29–36.
[3] J. Zheng, Y. Zhang, D. Hou, Y. Qin, W. Guo, C. Zhang, J. Shi, A review of nondestructive examination technology for polyethylene pipe in nuclear power plant, Front. Mech. Eng. 13 (2018) 535–545.
[4] A. Geringer, Active reinforcement for PE- electrofusion couplers/OFF-takes ON large-diameter PE mains, Proc. 17th Plast. Pip. Conf. PPXVII (2014). Illinois.
[5] ASME Boiler and Pressure Vessel Committee, ASME B&PV Code Case N-755-3: Use of Polyethylene (PE) Class 3 Plastic Pipe, Section III, Division I and Section XI, 2015 edition, ASME, New York, 2015.
[6] K. Chaoui, R. Khelif, N. Zeghib, A. Chateauneuf, Failure Analysis of Polyethylene Gas Pipes, Springer Netherlands, Dordrecht, 2008, pp. 131–163.
[7] K. Peterson, HDPE pipe for corrosion- and leak-free operation, ASHRAE J 59 (2017) 54–58.
[8] J.S. Kim, Y.J. Oh, S.W. Choi, C. Jang, Investigation on the thermal butt fusion performance of the buried high density polyethylene piping in nuclear power plant, Nucl. Eng. Technol. 51 (2019) 1142–1153.
[9] K.Q. Nguyen, C. Mwiseneza, K. Mohamed, P. Cousin, M. Robert, B. Benmokrane, Long-term testing methods for HDPE pipe - advantages and disadvantages: a review, Eng. Fract. Mech. 246 (2021) 107629–107644.
[10] J. Zheng, D. Hou, W. Guo, X. Miao, Y. Zhou, J. Shi, Ultrasonic inspection of electrofusion joints of large polyethylene pipes 138, 2016, 060908-060918.
[11] H. Chen, R.J. Scavuzzo, T.S. Srivatsan, Influence of joining on the fatigue and fracture behavior of high density polyethylene pipe, J. Mater. Eng. Perform. 6 (1997) 473–480.
[12] B.Y. Lee, J.S. Kim, S.Y. Lee, Y.K. Kim, Butt-welding technology for double walled Polyethylene pipe, Mater. Des. 35 (2012) 626–632.
[13] J. Bowman, A review of the electrofusion joining process for polyethylene pipe systems, Polym. Eng. Sci. 37 (1997) 674–691.
[14] Z. Chebbo, M. Vincent, A. Boujlal, D. Gueugnaut, Y. Tillier, Numerical and experimental study of the electrofusion welding process of polyethylene pipes, Polym. Eng. Sci. 55 (2015) 123–131.
[15] T. Cender, A. Lévy, S. Le Corre, Continuous Fusion Bonding of High Temperature Thermoplastic Composite Structures with Volumetric Heating, ICMAC Conf., Nottingham, 2018.
[16] V. Kovačević, Surface and interface phenomenon in polymers, Zagreb, Int. Cent. Ft. Theor. Phys. (2008).
[17] R.G. Stacer, H.L. Schreuder-Stacer, Time-dependent autohesion, Int. J. Fract. 39 (1989) 201–216.
[18] ISO 13953:2001 Polyethylene (PE) Pipes and Fittings — Determination of the Tensile Strength and Failure Mode of Test Pieces from a Butt-Fused Joint, International Organization for Standardization, 2001.
[19] ISO 21751:2011 Plastics Pipes and Fittings — Decohesion Test of Electrofusion Assemblies — Strip-Bend Test, International Organization for Standardization, 2011.
[20] ASTM D1599-18 Standard Test Method for Resistance to Short-Time Hydraulic Pressure of Plastic Pipe, Tubing, and Fittings, ASTM International, 2018.
[21] ASTM F2634-07 Standard Test Method for Laboratory Testing of Polyethylene (PE) Butt Fusion Joints Using Tensile-Impact Method, ASTM International, 2007.
[22] ASTM F3183-16 Standard Practice for Guided Side Bend Evaluation of Polyethylene Pipe Butt Fusion Joint, ASTM International, 2016.
[23] D.J. Shim, P. Krishnaswamy, E. Focht, Comparison of parent and butt fusion material properties of high density polyethylene, in: Vessel. Pip. Conf., ASME 2009 Press, Maryland, 2009.
[24] T.M.A.A. El-Bagory, M.Y.A. Younan, H.E.M. Sallam, Mechanical behavior of welded and un-welded polyethylene pipe materials, in: Vessel. Pip. Conf., ASME 2013 Press, Paris, 2013.
[25] K. Leskovics, M. Kollár, P. Bárczy, A study of structure and mechanical properties of welded joints in polyethylene pipes, Mater. Sci. Eng. 419 (2006) 138–143.
[26] H.S. Lai, N.N. Tun, S.H. Kil, K.B. Yoon, Effect of defects on the burst failure of butt fusion welded polyethylene pipes, J. Mech. Sci. Technol. 30 (2016) 1973–1981.
[27] J.A. Cholewa, R.W.I. Brachman, I.D. Moore, Axial stress-strain response of HDPE from whole pipes and coupons, J. Mater. Civ. Eng. 23 (2011) 1377–1386.
[28] C. Fisher, G. Quesada, Tensile testing of a push-on restrained joint PVC pipe, J. ASTM Int. 8 (2011) 102855–102870.
[29] M. Troughton, C. Brown, J. Hessel, M. Piovano, Comparison of long-term and short-term tests for electrofusion joints in PE pipes, in: Plast. Pip. XIII conf., Washington, D.C., 2006.
[30] https://www.admet.com/products/engineered-solutions/horizontal-pipe-tensile-tester/, (Accessed 1st Dec 2020).

[31] J. Wermelinger, O. Hein, Long Term Influence of Defects in Butt Fusion Joints on PE100 Pipes and NDT Detection of Them, Proc. 18th Plast. Pip. Conf. PPXVIII, Berlin, 2016.
[32] S. Choi, ISO/TC138/SC5/WG17 N208, in: HAT Presentation, 2017. Solothurn.
[33] S. Choi, Understanding Long-Term Test on Butt-Fusion Joint, ASME BPV III meeting, St. Louis, 2016.
[34] S. Choi, H. Lim, J. Kim, K. Ahn, HDPE Pipe Fusion Jointing and Non-destructive Evaluation Method Development for Nuclear Power, Final Report-20131510200400, Nuclear Power Core Technology Development Program of the KETEP, 2017. Korea.
[35] S. Choi, Surface Embrittlement of Polyethylene, Ph.D. Thesis, Illinois institute of technology, 1992.
[36] S. Kut, State of stress identification in numerical modeling of 3D issues, Arch. Metall. Mater. 54 (2009) 627–632.
[37] T. Eom, Development of Notched Fusion Zone Tensile (NFZT) Specimen for Evaluating PE Butt Fusion, Master Thesis, Hannam University, 2021.
[38] W. Lee, Investigation of Creating Cold Fusion (CF) Defect in HDPE Fusion Joint, Master Thesis, Hannam University, 2021.
[39] M. Shaheer, Effects of Welding Parameters on the Integrity and Structure of HDPE Pipe Butt Fusion Welds, PhD. Thesis, Brunel University, 2017.